J|A|C|S
ARTICLES

Published on Web 10/20/2010

Controlled Plasmon Resonance Properties of Hollow Gold Nanosphere Aggregates

Manabendra Chandra, Anne-Marie Dowgiallo, and Kenneth L. Knappenberger, Jr.*

Department of Chemistry and Biochemistry, Florida State University, Tallahassee, Florida 32306, United States

Received August 12, 2010; E-mail: klk@chem.fsu.edu

Abstract: Hollow gold nanospheres (HGNs) ranging from 29.9 nm/8.5 nm (outer diameter/shell thickness) to 51.5 nm/4.5 nm and having aspect ratios spanning 3.5−11.7 were employed to investigate the ability to tailor charge oscillations of HGN aggregates by systematic variation of particle aspect ratio, interparticle gap, and nanosphere inner surface spatial separation. Altering these properties in aggregated HGNs led to control over the interparticle plasmon resonance. Thiol-mediated aggregation was accomplished using either ethanedithiol or cysteine, resulting in dimeric structures in which monomer subunits were spatially separated by <3 Å and 1.2 ± 0.7 nm, respectively. Particle dimensions and separation distances were confirmed by transmission electron microscopy. Experimental absorption spectra obtained for high-aspect ratio nanospheres dimerized using ethanedithiol exhibited an obvious blue shift of the surface plasmon resonance (SPR) relative to that observed for the native, monomeric HGN. This spectral difference likely results from a charge-transfer plasmon resonance at the dimer interface. The extent of the blue shift was dependent upon shell thickness. Dimers comprised of thin-shelled HGNs exhibited the largest shift; aggregates containing HGNs with thick shells (≥ 7 nm) did not display a significant SPR shift when the individual particles were in contact. By comparison, all cysteine-induced aggregates examined in this study displayed large interparticle gaps (>1 nm) and a red-shifted SPR, regardless of particle dimensions. This effect can be described fully by a surface mode coupling model. All experimental measurements were verified by finite difference time domain calculations. In addition, simulated electric field maps highlighted the importance of the inner HGN surface in the interparticle coupling mechanism. These findings, which describe structure-dependent SPR properties, may be significant for applications derived from the plasmonic nanostructure platform.

Introduction

Owing largely to surface plasmon resonance (SPR) phenomena, metal nanostructures represent a promising class of materials with size- and shape-tunable properties. Plasmon-supporting nanoparticles can be used to create devices capable of functioning throughout the visible and near-infrared electromagnetic regions. The combination of facile laboratory synthesis[1−4] and elegant "superstructure" assembly techniques[5−10] has stimulated expectations of superior products in fields such as photovoltaics,[11] biological labels,[12] nonlinear optics,[13] three-dimensional waveguides,[14] and negative refractive index materials.[15] However, the influence of the precise arrangement of plasmonic nanoparticles within a designed array on the collective properties of composite materials must be understood before many of these applications can be realized. In this paper, we present experimental and computational data that demonstrate control over the SPR spectral position and electric field spatial distribution of hollow gold nanospheres (HGNs). This was

(1) Oldenburg, S.; Averitt, R. D.; Westcott, S.; Halas, N. J. *Chem. Phys. Lett.* **1998**, *288*, 243.
(2) (a) Schwartzberg, A. M.; Olson, T. Y.; Talley, C. E.; Zhang, J. Z. *J. Phys. Chem. B* **2006**, *110*, 19935. (b) Schwartzberg, A. M.; Zhang, J. Z. *J. Phys. Chem. C* **2008**, *112*, 10323.
(3) Gole, A.; Murphy, C. J. *Chem. Mater.* **2004**, *16*, 3633.
(4) El-Sayed, M. A. *Acc. Chem. Res.* **2001**, *34*, 257.
(5) Nishida, N.; Shibu, E.; Yao, H.; Oonishi, T.; Kimura, K.; Pradeep, T. *Adv. Mater.* **2008**, *20*, 4719.
(6) Chen, C. L.; Rosi, N. L. *J. Am. Chem. Soc.* **2010**, *132*, 6902.
(7) Chen, C. L.; Zhang, P.; Rosi, N. L. *J. Am. Chem. Soc.* **2008**, *130*, 13555.
(8) Rosi, N. L.; Thaxton, C. S.; Mirkin, C. A. *Angew. Chem., Int. Ed.* **2004**, *43*, 5500.
(9) Payne, E. K.; Rosi, N. L.; Xue, C.; Mirkin, C. A. *Angew. Chem., Int. Ed.* **2005**, *44*, 5064.
(10) Chang, W. S.; Slaughter, L. S.; Khanal, B. P.; Zubarev, E. R.; Link, S. *Nano Lett.* **2009**, *9*, 1152.
(11) (a) Pryce, I. M.; Koleske, D. D.; Fischer, A. J.; Atwater, H. A. *Appl. Phys. Lett.* **2010**, *96*, 153501. (b) Saeta, P. N.; Ferry, V. E.; Pacifici, D.; Munday, J. N.; Atwater, H. A. *Opt. Express* **2009**, *17*, 20975.
(12) (a) Ray, P. C.; Darbha, G. K.; Ray, A.; Walker, J.; Hardy, W.; Perryman, A. *Plasmonics* **2007**, *2*, 1730183. (b) Griffin, J.; Ray, P. C. *J. Phys. Chem. B* **2008**, *112*, 11198.
(13) (a) Masia, F.; Langbein, W.; Watson, P.; Borri, P. *Opt. Lett.* **2009**, *34*, 1816. (b) Jung, Y.; Chen, H.; Tong, L.; Cheng, J. X. *J. Phys. Chem. C* **2009**, *113*, 2657. (c) Chandra, M.; Dowgiallo, A. M.; Knappenberger, K. L., Jr. *J. Phys. Chem. C* **2010**, submitted.
(14) (a) Maier, S. A.; Kik, P. G.; Atwater, H. A.; Meltzer, S.; Harel, E.; Koel, B. E.; Requicha, A. A. G. *Nat. Mater.* **2003**, *2*, 229. (b) Lindquist, N. C.; Nagpal, P.; Lesuffleur, A.; Norris, D. J.; Oh, S. H. *Nano Lett.* **2010**, *10*, 1369.
(15) (a) Urzhumov, Y. A.; Shvets, G.; Fan, J.; Capasso, F.; Brandl, D.; Nordlander, P. *Opt. Express* **2007**, *15*, 14129. (b) Dionne, J. A.; Verhagen, E.; Polman, A.; Atwater, H. A. *Opt. Express* **2008**, *16*, 19001. (c) Nagpal, P.; Lindquist, N. C.; Oh, S. H.; Norris, D. J. *Science* **2009**, *325*, 5940.

10.1021/ja106910x

accomplished using judicious thiol-induced aggregation to form structures that contain only a few HGNs. Surprisingly, the surface plasmon spectral position could be tuned to either higher or lower frequencies, depending upon the size of the interparticle separation and the HGN shell thickness. Moreover, numerical results, which were consistent with the experimental data, indicated that the resultant electric field amplitude and spatial distribution achieved using HGN aggregates could be tailored by altering the dimensions of the individual nanospheres comprising the aggregate.

We recently reported the experimental observation of an aggregation-induced blue shift of the surface plasmon resonance of HGNs.[16] HGNs,[2] like dielectric core−shell nanoparticles,[1,17] can be used to extend the functional range of devices on the basis of the plasmonic platform; the SPR can be tuned across the visible and NIR spectral regions by changing the aspect ratio (outer diameter:shell thickness) of the gold sphere. HGNs are synthesized by a sacrificial template method in which the atoms of a cobalt nanosphere are exchanged for gold, forming a hollow plasmon-supporting gold shell with inner and outer surfaces.[2,16,18] This galvanic replacement mechanism, similar to electrodeposition processes, restricts the growth of the nanosphere to thicknesses that are typically less than 10 nm.[2] As a result, HGNs can be used to study collective processes that arise when the interior (cavity) surfaces of a nanostructure are separated by very small distances. In addition, the role of each surface in interparticle plasmonics can be determined by systematically varying the spatial separation of the inner (outer) surfaces.

Electromagnetic surface fields formed by the interaction of nanospheres and nanorods have created significant interest among both experimentalists and theoreticians.[16,19−28] It is well known that, when nanospheres aggregate in such a manner that a large (>1 nm) interparticle gap exists between the monomeric subunits, they exhibit a large and unstructured spectral red shift of the plasmon resonance.[20,23] This experimental observation has been satisfactorily described as a bonding hybridized plasmon resonance mode.[23] However, a detailed description of the interactions between nanostructures that are either in extreme proximity or in contact with each other is still needed. As we reported previously, the SPR of aggregated surface-necked HGNs is shifted to shorter wavelengths than the transverse SPR of an isolated HGN.[16] Finite difference time domain simulations suggest the blue-shifted SPR can be assigned to newly formed longitudinal SPR of HGN dimers. Two possible explanations for this surprising SPR blue shift are (a) antibonding modes of hybridized plasmons of HGN dimers[22] or (b) a charge-transfer plasmon resonance.[24−26] In the first case, a SPR blue shift would be observed for an asymmetric nanosphere aggregate when spectral weight is transferred from the lower-frequency bonding mode to the higher-frequency antibonding hybrid mode, or other higher-order modes.[23] In the case of the charge-transfer model,[25,26] a blue shift would be expected when the particles are either in contact or separated by distances short enough to permit a conductive overlap; such an overlap would lead to a collective time-dependent charge oscillation over the two particles comprising the dimer.

In the current study, we used thiol linkages to form small aggregates such as nanosphere dimers, trimers, and tetramers, as well as larger extended structures that can be used to elucidate key parameters that influence collective charge oscillations in plasmonic assemblies. Our findings indicated that HGNs can exhibit both hybridized plasmon modes and collective charge-transfer resonances when the particles are assembled into small or large extended aggregate structures. The interparticle gap and shell thickness were identified as key factors that influenced aggregate optical properties. When aggregates containing significant interparticle spatial separation were created, a dielectric gap was formed that screened the two particles. In this case, the optical response was fully described by the hybridization of surface plasmon modes. In contrast, negligible interparticle gaps led to a domination of the visible absorption spectra by charge-transfer resonances.

Experimental Methods

HGNs having outer diameters ranging from 30 to 55 nm and shell thicknesses of 4.5−8.6 nm (resulting outer-diameter-to-shell-thickness aspect ratios were between 3.5 and 11.7) were synthesized using a sacrificial galvanic replacement method.[2,16] A detailed synthetic protocol for each HGN system is provided in the Supporting Information. Two different inducers of thiol-mediated nanosphere aggregation were employed: ethanedithiol and cysteine. For ethanedithiol syntheses, 2 μL portions of a 5 mM solution of ethanedithiol in ethanol were injected into 1 mL of each HGN solution. The solution was agitated by shaking and then allowed to equilibrate at room temperature for 1 h before performing experiments. For preparing cysteine-based HGN aggregates, 10 μL portions of 1 M aqueous solution of cysteine were added to 1 mL of each HGN solution.

Isolated and aggregated HGNs were characterized by absorption spectroscopy and transmission electron microscopy (TEM). Absorption data were collected using a Perkin-Elmer (Lambda 950) absorption spectrometer. TEM images were recorded on an FEI CM-120 transmission electron microscope at an acceleration voltage of 120 kV. Samples were added to a Formvar-coated copper grid and then air-dried for 24 h prior to TEM data collection.

Computational Methods

The absorption spectra of all experimentally studied HGNs and their dimers (at distinct interparticle distances) were numerically simulated using the finite difference time domain (FDTD) technique.[29] Simulations were performed using FDTD Solutions software from Lumerical. Absorption spectra of HGNs and HGN dimers were simulated using 2 nm mesh and an environmental dielectric constant of unity. The material dielectric constants were

(16) Knappenberger, K. L., Jr.; Schwartzberg, A. M.; Dowgiallo, A. M.; Lowman, C. A. *J. Am. Chem. Soc.* **2009**, *131*, 13892.
(17) (a) Wang, H.; Brandl, D. W.; Nordlander, P.; Halas, N. J. *Acc. Chem. Res.* **2007**, *40*, 53. (b) Prodan, E.; Nordlander, P. *J. Chem. Phys.* **2004**, *120*, 5444.
(18) Liang, H. P.; Wan, L. J.; Bai, C. L.; Jiang, L. *J. Phys. Chem. B* **2005**, *109*, 7795.
(19) Zou, S.; Janel, N.; Schatz, G. C. *J. Chem. Phys.* **2004**, *120*, 10871.
(20) Jain, P. K.; Eustis, S.; El-Sayed, M. A. *J. Phys. Chem. B* **2006**, *110*, 18243.
(21) Grant, C. D.; Schwartzberg, A. M.; Norman, T. J.; Zhang, J. Z. *J. Am. Chem. Soc.* **2003**, *125*, 549.
(22) Romero, I.; Aizpurua, J.; Bryant, G. W.; Garcia de Abajo, F. J. *Opt. Express* **2006**, *14*, 9988.
(23) Lassiter, J. B.; Aizpurua, J.; Hernandez, L. I.; Brandl, D. W.; Romero, I.; Lal, S.; Hafner, J. H.; Nordlander, P.; Halas, N. J. *Nano Lett.* **2008**, *8*, 1212.
(24) Zuloaga, J.; Prodan, E.; Nordlander, P. *Nano Lett.* **2009**, *9*, 887.
(25) Wu, Y.; Nordlander, P. *J. Phys. Chem. C* **2010**, *114*, 7302.
(26) Malynych, S.; Chumanov, G. *J. Am. Chem. Soc.* **2003**, *125*, 2896.
(27) (a) Mahmoud, M.; El-Sayed, M. A. *Nano Lett.* **2009**, *9*, 3025. (b) Jain, P. K.; El-Sayed, M. A. *Chem. Phys. Lett.* **2010**, *487*, 153.
(28) Slaughter, L. S.; Wu, Y.; Willingham, B. A.; Nordlander, P.; Link, S. A. *ACS Nano* **2010**, *4*, 4657.
(29) Oubre, C.; Nordlander, P. *J. Phys. Chem. B* **2005**, *109*, 10042.

Table 1. Outer Diameters, Shell Thicknesses, Aspect Ratios (Outer Diameter-to-Shell Thickness Ratio), and SPR Peak Positions of All the Isolated HGNs Studied in This Work

HGNs	outer diameter (nm)	shell thickness (nm)	aspect ratio	SPR (nm)	$\Delta\lambda = (\lambda_{dimer} - \lambda_{HGN})^a$ (nm)
HGN-I	31.20(±4.60)	6.30(±2.06)	5.37(±1.51	577	−9
HGN-II	29.90(±6.15)	8.48(±2.17)	3.53(±0.61)	548	+4
HGN-III	54.76(±12.24)	6.86(±1.62)	8.26(±2.25)	647	−10
HGN-IV	53.32(±10.48)	5.70(±0.99)	9.53(±2.07)	658	−9
HGN-V	49.28(±9.66)	5.07(±0.81)	9.85(±1.96)	695	−47
HGN-VI	51.49(±7.80)	4.52(±0.79)	11.69(±2.53)	713	−26
HGN-VII	54.57(±12.46)	8.57(±2.85)	6.71(±1.84)	608	0

[a] SPR peak shifts of the HGNs upon ethanedithiol addition.

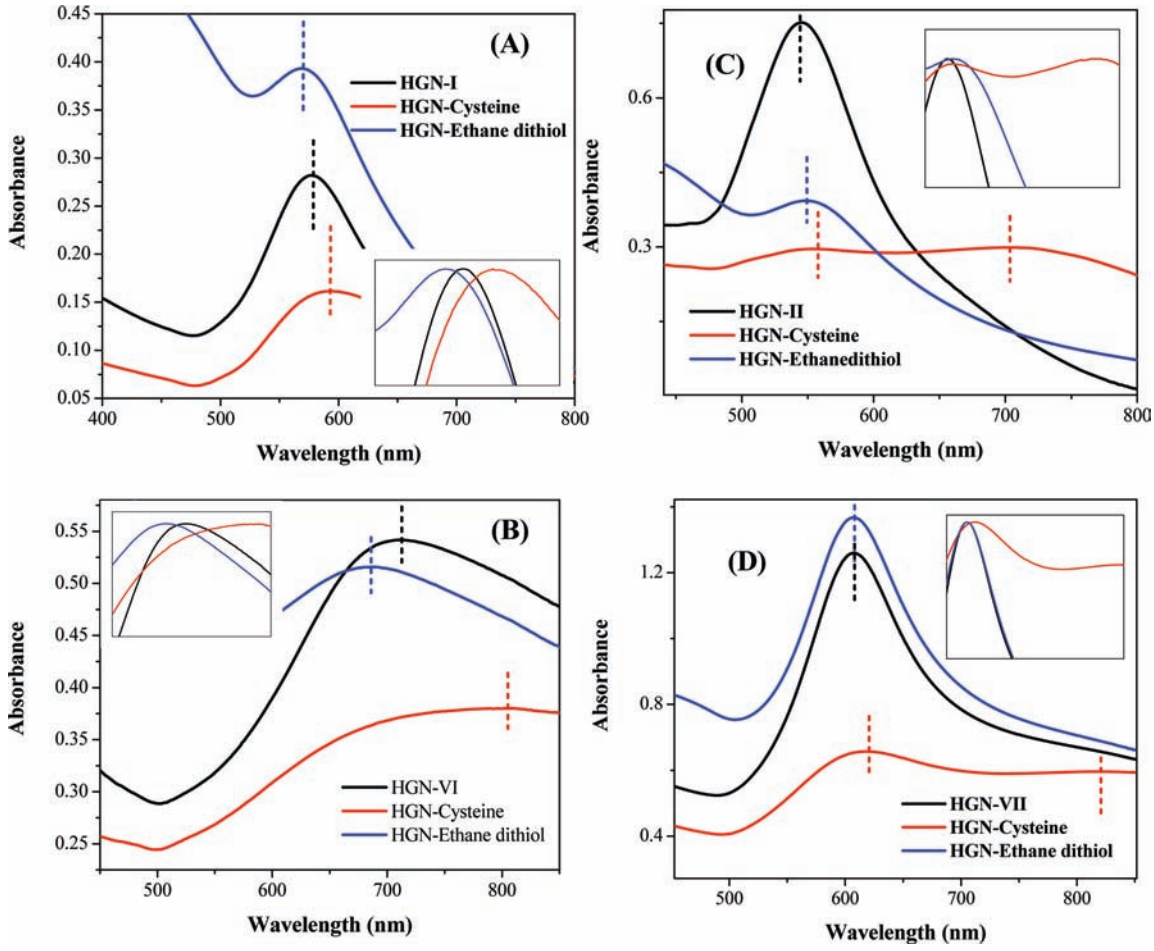

Figure 1. Experimental absorption spectra comparing isolated HGN and HGN aggregates induced by ethanedithiol and cysteine. Dashed straight lines are provided as guides to the absorption peaks. Addition of ethanedithiol resulted in a distinct blue shift of the SPR for HGNs having shell thickness less than 7 nm (A,B) and a small red shift or no peak shift for HGNs with shell thickness greater than 7 nm (C,D). Truncated spectra (normalized at respective SPR maxima) of all the HGNs and their aggregates are provided as insets to show the peak shifting more clearly.

taken from Johnson and Christy.[30] In the case of HGN dimers, the incident electromagnetic field was polarized parallel to the interparticle axis.

Results and Discussion

In order to study the structure dependence of interparticle coupling, we synthesized two groups of HGNs: particles with an outer diameter of approximately 30 nm and particles having an outer diameter of ≥50 nm. Shell thicknesses for both particle classes were varied to generate HGNs with controlled aspect ratios, enabling investigation of the role of hollow particle dimensions in interparticle plasmon coupling. Dimensions, along with their standard deviations, for all HGNs investigated are provided in Table 1. Two different types of aggregate structures were achieved: (i) contact HGN dimers and (ii) spatially separated HGN dimers with a >1 nm interparticle gap. Contact HGN dimers were formed by ethanedithiol-induced aggregation; cysteine was used for the spatially separated dimers. Normalized absorption spectra of four representative HGNs, along with their aggregate structures, are shown in Figure 1. Spectral positions of peaks observed for the colloidal HGNs are summarized in Table 1. The SPR spectral position seen for isolated HGNs depends directly on the diameter/shell thickness aspect ratio. For all seven dimensions of HGNs examined in this study, cysteine addition yielded an absorption spectrum that was broader and red-shifted relative to that observed for isolated

(30) Johnson, P. B.; Christy, R. W. *Phys. Rev. B* **1972**, *6*, 4370.

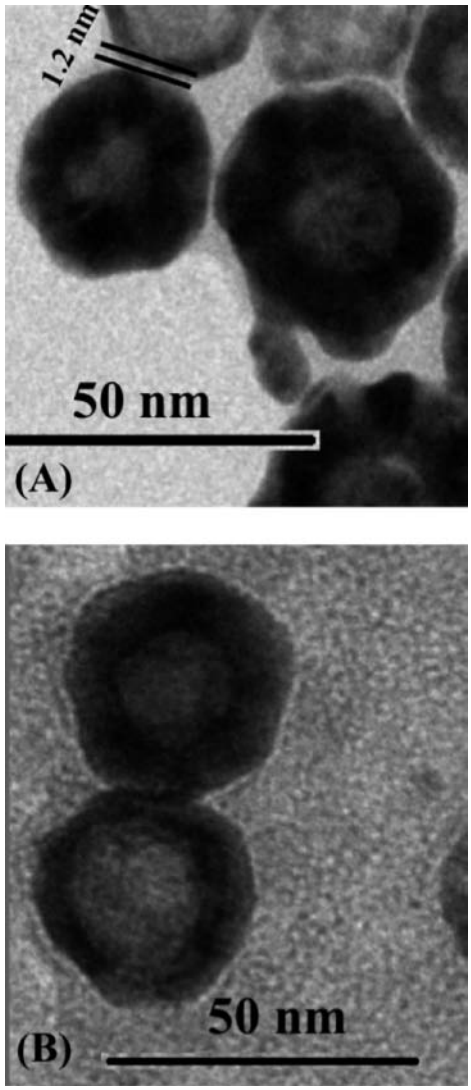

Figure 2. TEM images comparing two different aggregate structures of HGN-I. (A) Cysteine-induced aggregate and (B) dithiol-induced aggregate. Scale bars correspond to 50 nm. Interparticle gaps are quite obvious in the cysteine-induced aggregates, while dithiol-induced dimers showed no interparticle separation.

HGNs (Figure 1). This observation was consistent with previous work on cysteine-mediated aggregation of solid gold nanoparticles.[31] By comparison, addition of ethanedithiol to the HGN dispersion resulted in distinct blue shifts of the SPR for all particles having a shell thickness <7 nm (Figure 1A,B). For HGNs with thicker shells, ethanedithiol addition led to either no peak shift or a small red shift with almost no change in the spectral bandwidth (Figure 1C,D)—even extension of the spectrum to 1200 nm revealed no additional absorption peaks. Truncated spectra are shown as Figure 1 insets to highlight the effect of the aggregation agent on optical properties.

The HGN aggregates were structurally characterized using TEM analysis following either cysteine or ethanedithiol addition. TEM images (Figure 2) clearly demonstrated that addition of cysteine and ethanedithiol to the colloidal HGN solutions resulted in two different structures. Cysteine addition led to the formation of large, extended aggregates, whereas the addition

Scheme 1. Probable Motif of Cysteine-Induced Aggregation of HGNs (not to scale)

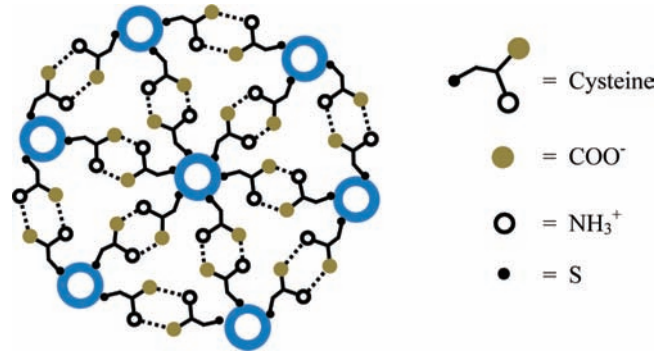

of ethanedithiol yielded small aggregates comprised primarily of dimers, trimers, and tetramers. The statistical distribution of aggregate sizes (e.g., dimers, trimers, etc.) formed after ethanedithiol addition to the HGNs was also determined. Approximately 40−50% of the HGNs in solution aggregated upon ethanedithiol treatment. Of these, most (30% of $[HGN]_{total}$) were found in dimeric structures. Statistical histograms of these data are provided in the Supporting Information. We note that cysteine-induced aggregation could also be controlled to restrict the aggregate size to a few nanospheres by keeping the cysteine concentration and volume low (2 μL, 5 mM), as was done for addition of ethanedithiol. Even in this case, though, cysteine-induced HGN aggregates exhibited a small red shift of the SPR (Supporting Information). A striking difference between the particles produced using the two types of thiol-mediated aggregation was the resulting spatial separation of the monomers forming the aggregate. The average interparticle distance of cysteine-induced aggregates was approximately 1.2 ± 0.7 nm (complete statistics available in Supporting Information). In contrast, HGN aggregates formed using ethanedithiol were either in or near contact, making them within the conductive limit of the gold spheres.[27] The results presented in Figures 1 and 2 clearly demonstrate that the use of two different ligands (i.e., cysteine and ethanedithiol) allows for control over the aggregate structure and, in turn, the optical properties of the HGN aggregate. We note that, although the isolated HGN precursors have a distribution of sizes, for a given sample the optical properties were dictated by the interparticle spatial separation.

Cysteine is known to induce extended aggregation in solid nanoparticles through the formation of a hydrogen bond network, as shown in Scheme 1.[32] In fact, the measured interparticle distance of $\sim 1.2 \pm 0.7$ nm approximates the length of two cysteine molecules bonded via intermolecular hydrogen bonding. FTIR measurements (Supporting Information) of the cysteine-induced HGN aggregates supported this type of hydrogen-bonding scheme. The FTIR spectra observed for the aggregated samples no longer included the S−H stretching vibrational mode at 2564 cm^{-1}.[33] The disappearance of this vibration indicated Au−S bond formation, which results in loss of the thiolic proton. The band at 3274 cm^{-1}, which corresponds to N−H stretching,[33] was significantly broadened, suggesting hydrogen bonding of the amide proton. Taken together, the TEM structural characterization and the FTIR vibrational analysis

(31) Mocanu, A.; Cernica, I.; Tomoaia, G.; Bobos, L. D.; Horovitz, O.; Tomoaia-Cotisel, M. *Colloids Surf. A* **2009**, *338*, 93.

(32) Mandal, S.; Gole, A.; Lala, N.; Gonnade, R.; Ganvir, V.; Sastry, M. *Langmuir* **2001**, *17*, 6262.

(33) Wang, J.; Li, Y. F.; Huang, Z.; Wu, T. *Anal. Chim. Acta* **2008**, *626*, 3743.

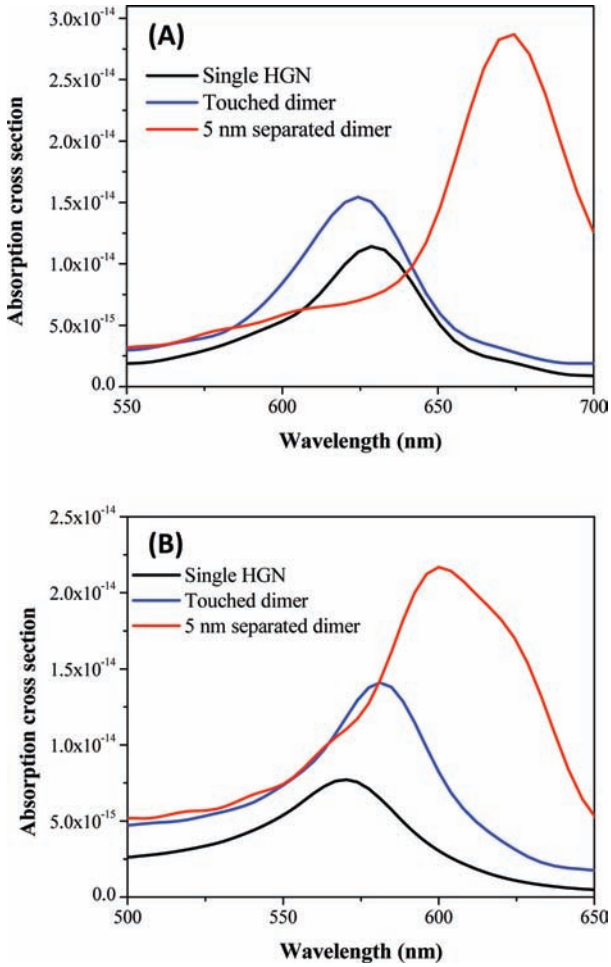

Figure 3. FDTD simulated absorption spectra of 53 nm HGN with shell thickness of (A) 5 nm and (B) 8 nm. Panels A and B closely mimic the experimental results presented in Figure 1, panels B and D.

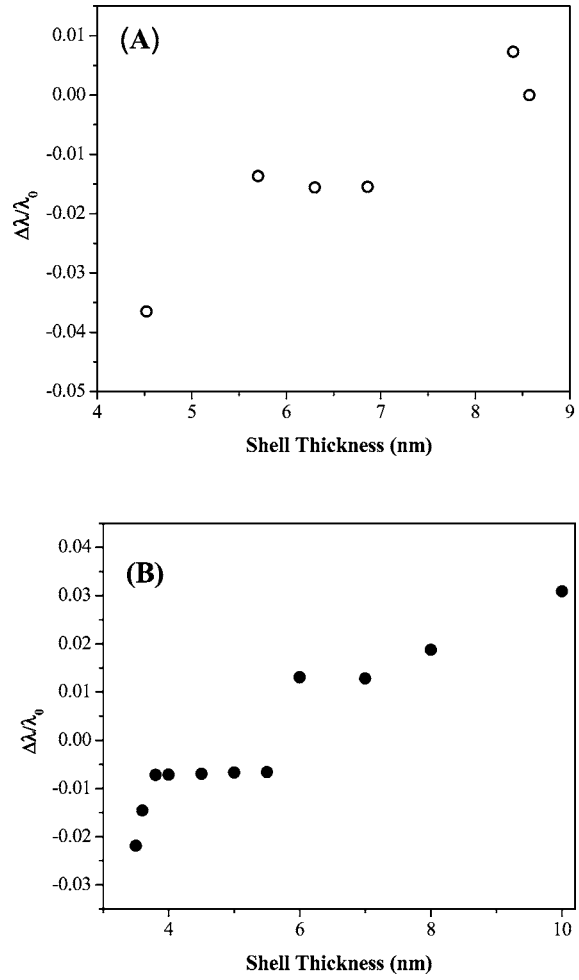

Figure 4. Plot of $\Delta\lambda/\lambda_0$ (normalized peak shift) as a function of HGN shell thickness. (A) Experimental results obtained for ethanedithiol-induced HGN aggregates (B) FDTD simulated results for "contact" HGN dimers. The HGN outer diameter was fixed at 53 nm in the simulation.

supported the mechanism presented in Scheme 1 for aggregates induced by cysteine addition. However, the structure of the small aggregates induced by ethanedithiol was clearly different. For these particles, the terminal sulfur atoms of ethanedithiol may coordinate to gold surface atoms of a single HGN, or the molecule may form a bridge between two HGNs.[34] In either case, the nanospheres comprising the dimers or other small aggregates obtained in the presence of ethanedithiol would be in contact or separated by a very subtle gap ($\leq$3 Å). This small spatial separation is within the conductive limit of the gold nanospheres.[24,28]

To understand better the relationship between aggregate structure and the direction (red or blue) of the spectral shift, we used FDTD calculations to simulate the absorption spectra of two types of HGN aggregate structures: those with interparticle gaps and those that are in contact. HGN dimers were chosen as a simple, yet appropriate, model for aggregated structures. The simulated spectra (Figure 3) for 53 nm HGNs (with various shell thicknesses) and their two different dimers (in contact and separated by a 5 nm gap) qualitatively reproduced our experimental data. Figure 3 presents calculations for samples with shell thicknesses of 5 and 8 nm. A red shift of the SPR was observed for HGN dimers separated by a 5 nm interparticle gap, regardless of shell thickness. This numerical result was consistent with our experimental absorption measurements on aggregates formed using cysteine, in which the interparticle gap was 1.2 $\pm$ 0.7 nm. These findings indicated that modes associated with the outer surface were the dominant contributors to interparticle coupling for spatially separated particles.

Dimers formed by placing HGNs in contact (as with the ethanedithiol method) exhibited a spectral response that was strongly dependent upon the shell thickness of the HGN monomer. A small red shift of the simulated SPR peak was observed for systems comprised of HGNs with thick (8 nm) shells; a blue shift was obtained for thinner-shell HGNs (e.g., 5 nm). The extent of the spectral blue shift increased sharply with further reduction of the shell thickness (<4 nm), in exact agreement with our experimental measurements. This effect is illustrated in Figure 4, where both experimental and calculated relative spectral shifts ($\Delta\lambda/\lambda_0$) are plotted as a function of shell thickness to depict the transition from red-shifted to blue-shifted SPR in contact dimers. The influence of shell thickness on the SPR frequency suggested significant interaction between the cavity modes of two HGNs with shell thicknesses below a critical value. The influence of HGN shell thickness on dimer plasmon properties was also evident in the simulated electric field spatial profiles, shown in Figure 5. Nanostructure electric fields were simulated for HGNs having an outer diameter of 53 nm and shell thicknesses of 5, 7, and 10 nm. Electric field

(34) Joo, S. W.; Han, S. W.; Kim, K. *Langmuir* **2000**, *16*, 5391.

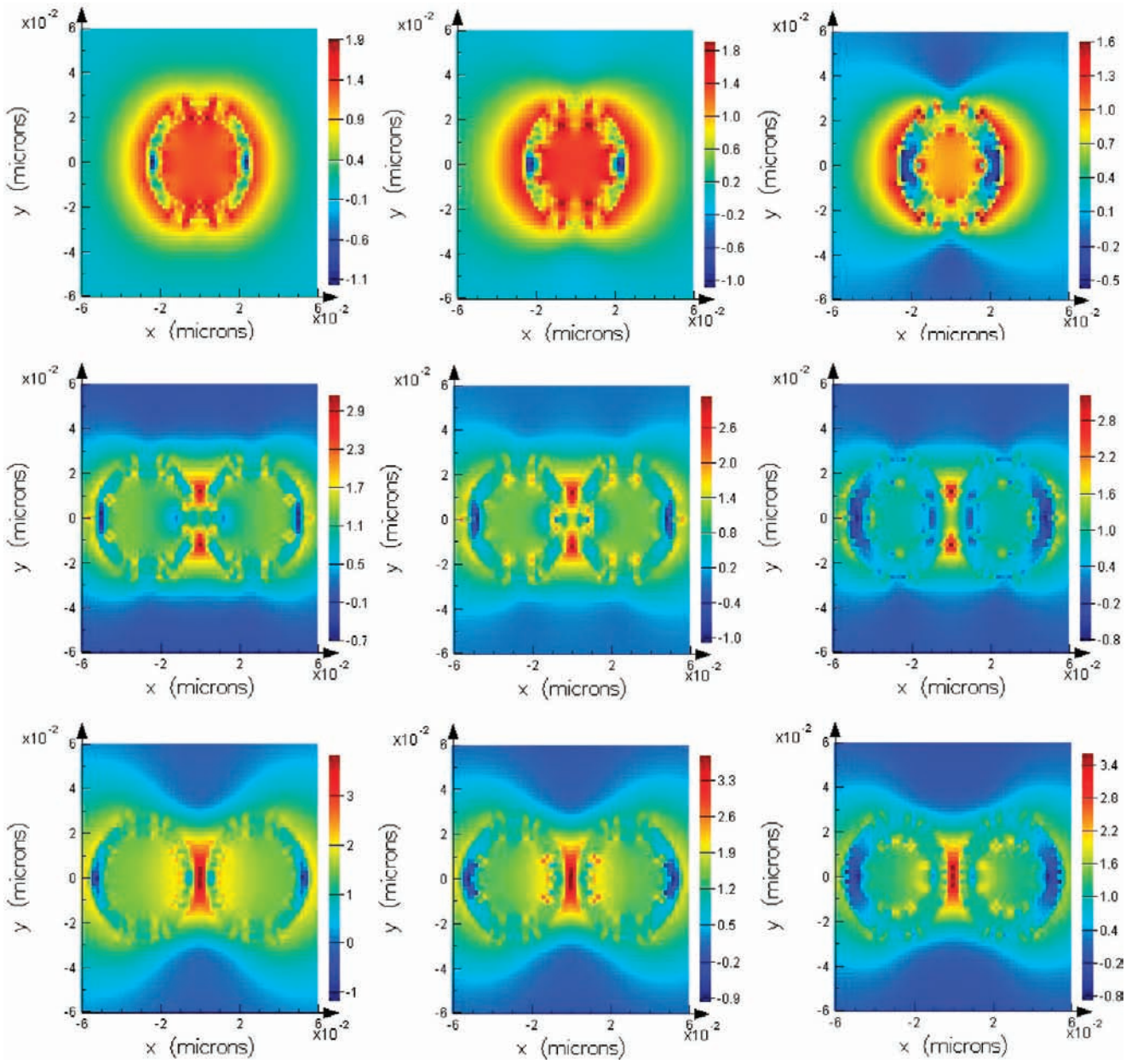

Figure 5. Electric field maps at various shell thicknesses: from left to right in each panel, 5, 7, and 10 nm. The top panels are for a single HGN, the middle panels are for contact dimers, and the bottom panels are for HGN dimers with a 5 nm interparticle gap. The outer diameter of these HGNs was 53 nm.

maps in Figure 5 correspond to isolated HGNs, dimers in contact, and dimers in which the component monomers are separated by a 5 nm gap. As can be seen in Figure 5 (left column, middle row), a significant electric field was observed along cavity walls for contact HGNs with 5 nm shells. In contrast, HGNs with 10 nm shells exhibited the majority of the electric field intensity at the conical region at the particle interface (Figure 5, right column, middle row). Taken together, the experimental and numerical data indicate that cavity modes greatly influenced the plasmon properties of contacting HGNs. We note that HGN-V yielded a very large SPR blue shift upon aggregation with ethanedithiol (Table 1). However, unlike all of the other samples considered here, TEM images indicate that this structure included many surface defects and did not have a uniform gold shell. Therefore, we report the structural and optical properties in Table 1 for reference but do not consider them for our overall analysis.

Additionally, we investigated whether HGN shell thickness or aspect ratio was dominant in determining the direction (red or blue) of the SPR peak's spectral shift. The data detailing this comparison are found in Table 1. The absorption spectrum of HGN-I (31.2 nm/6.3 nm) displayed a distinct SPR blue shift upon ethanedithiol addition; by comparison, the SPR band in the HGN-VII (54.57 nm/8.57 nm) spectrum did not shift. The aspect ratios for HGN-VII and HGN-I were 6.71 and 5.37, respectively. If aspect ratio were the HGN property that controlled peak shift in contact dimers, then the trend in peak shift (for the HGNs-I and VII) should have been reversed because the lower aspect ratio species would be expected to behave more like a solid particle. In fact, we see no correlation between aspect ratio and SPR peak shift. HGN-I and HGN-VII also differed in shell thickness. HGN-I had a 6.30 nm wall, whereas the shell for HGN-VII was 8.57 nm thick. The spectral blue shift observed for HGN-I indicated that its thinner shell

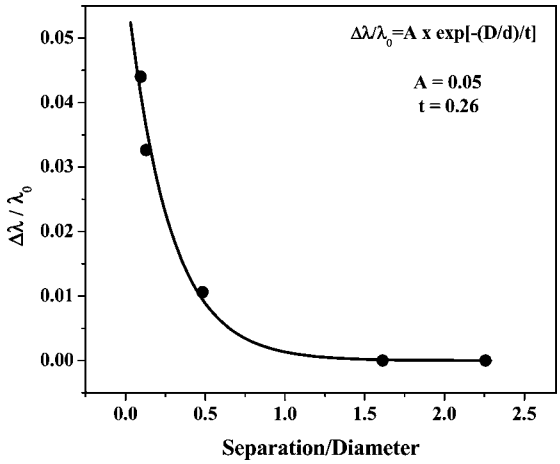

Figure 6. Plot of the simulated SPR peak shift (red shift $\Delta\lambda$ for spatially separated dimers; normalized by the SPR maximum of the isolated particle as $\Delta\lambda/\lambda_0$) as a function of interparticle gap to outer diameter ratio (D/d) for HGN-I. The obtained decay constant (t) value is consistent with that of the solid nanospheres of similar diameter.

allowed cavity modes to interact strongly with each other, despite HGN-I's lower aspect ratio. Owing to a larger distance between inner surfaces, this type of interaction would be weaker in a thick-shelled contact dimer, such as that comprised of HGN-VII monomers. Thus, it appeared that, in the case of contact or necked aggregates, shell thickness (rather than aspect ratio) dictated the direction of the SPR spectral shift.

The absorption spectra observed for cysteine-induced HGN aggregates have been explained by a hybridization model originally developed for both isolated and aggregated metal−dielectric core−shell particles.[22] Adopting this model for HGNs, outer surface plasmon modes (or, simply, surface plasmon modes) interact with inner surface (cavity) plasmon modes, yielding a symmetric low-energy bonding resonance and an antisymmetric high-energy antibonding state. The bonding plasmon (symmetric coupling between surface and cavity modes) has a large dipole moment and, therefore, has a larger absorption cross section than the antibonding plasmon. As a result, the absorption spectra of HGNs are red-shifted compared to their solid analogues of similar sizes, giving rise to spectrally tunable SPR of HGNs and core−shell nanospheres. Although the SPR energy levels of isolated HGNs hybridize via a coupling of surface and cavity plasmons, multiple combinations of distance-dependent hybridized modes become observable when two HGNs approach one another. In the case of symmetric HGN homodimers, multiple types of interactions involving surface and cavity plasmons may exist: surface plasmon(1)−surface plasmon(2), cavity plasmon(1)−cavity plasmon(2), and other, higher-order modes. Typically, the symmetric bonding mode dominates aggregate absorption, giving rise to red-shifted peaks extending into the NIR.[20,22−28] The assembly of asymmetric heterodimers from nanoparticles of different dimensions can reduce symmetry and yield multiple SPR peaks.[28]

In the case of cysteine-induced aggregates with substantial interparticle gaps, a large SPR red shift and concomitant band broadening were observed. This observation was consistent with the symmetric surface plasmon(1)−surface plasmon(2) hybridization model described above, a behavior also observed for solid nanoparticle aggregates.[20] The simulated SPR spectral position as a function of HGN outer diameter (d) to interparticle gap (D) ratio is shown in Figure 6 for several of the HGN dimers studied here. These data indicate that HGN dimers exhibit the well-known "plasmon ruler" behavior of solid nanospheres, in which case a distance-dependent spectral shift of the dimer plasmon results.[35−37] This finding was consistent with the symmetric surface−surface coupling model used to describe HGN dimers having an interparticle gap. We attribute the large spectral red shift to dielectric screening effects that arise from the presence of cysteine in the gap separating HGN surfaces. At a ~1.2 nm interparticle gap, large dipolar coupling among surface plasmons appeared to localize the electric field to the space between particles. This behavior was verified by FDTD simulations (Figure 5, bottom row). The spectral broadening that accompanied the SPR red shift was consistent with large and extended aggregate structures, as observed in the electron microscope images (Figure 2B and Supporting Information).

By comparison, HGNs that were in or near contact, as was the case for ethanedithiol-induced aggregation, displayed complex plasmonic behavior. A complete description of touching HGNs requires consideration of at least three possible contributions: (1) decreased red shifting of the SPR resulting from reduced dielectric screening, (2) increased contributions from antibonding or higher-order modes, and (3) formation of a charge-transfer plasmon resonance.

First, the effects of dielectric screening were examined. If the dielectric constant of the embedding ethanedithiol matrix were a dominant factor, a lower-frequency SPR (spectral red shift) would have been observed (refractive index of ethanedithiol is 1.5589 and that of water is 1.33 at 20 °C).[38] This is contrary to both our experimental and numerical data on samples formed using ethanedithiol as an aggregating agent. Therefore, changes in dielectric screening alone cannot be used to account for the experimentally observed SPR blue shift of contact HGN pairs.

Next, we considered contributions from antibonding or higher-order modes. Thinner HGN shells allow for increased interaction between cavity and surface plasmons, thus resulting in a more dominant antibonding mode that gains spectral weight from the bonding mode.[22] Hybridized plasmon modes have been extensively studied.[22−28] When HGN dimers are formed (the simplest case of an aggregated structure), the plasmon modes of one particle can interact with those of the other particle. According to existing models, the hybridized bonding (or symmetric) mode and antibonding (or antisymmetric) mode of each HGN should couple to their counterparts to give rise to the hybridized states of the dimer.[23] Coupling involving only the bonding modes of two HGNs will always lower the energy of the symmetric modes of the dimer, causing a red shift of the SPR.[17b] In contrast, interaction of antibonding HGN modes will give rise to a symmetric dimer mode at a higher energy compared to monomeric HGN, resulting in a blue shift in the SPR. Involvement of higher multipoles in the inter-HGN interaction can result in the appearance of numerous absorption peaks at resonance frequencies that depend on the outer-diameter-to-shell-thickness aspect ratio and the interparticle spatial separation. These interactions become increasingly significant for heterodimers owing to reduced symmetry.[28] Although the structures reported here were homodimers, it is possible that sample polydispersity was significant enough to

(35) Reinhard, B. M.; Siu, M.; Agarwal, H.; Alivisatos, A. P.; Liphardt, J. *Nano Lett.* **2005**, *5*, 2246–2252.
(36) Reinhard, B. M.; Sheikholeslami, S.; Mastroianni, A.; Alivisatos, A. P. *Proc. Natl. Acad. Sci. U.S.A.* **2007**, *104*, 2667.
(37) Jain, P. K.; Huang, W.; El-Sayed, M. A. *Nano Lett.* **2007**, *7*, 2080.
(38) LideD. R., Ed.; *CRC Handbook of Chemistry and Physics*, 90th ed.; CRC Press, Taylor & Francis Publishing Group: Boca Raton, FL, 2009−2010.

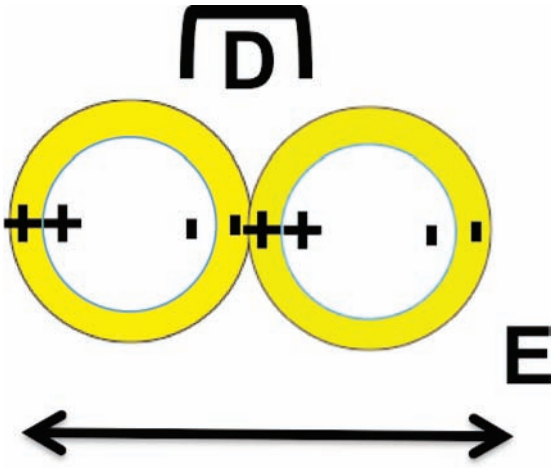

Figure 7. Schematic representation of a stable charge-transfer plasmon configuration. The incident electromagnetic field is polarized parallel to the interparticle axis of the hollow gold nanospheres. The combined interfacial shell thickness is given by *D*.

reduce symmetry. However, experimental observation of a single SPR band upon surface contact was not consistent with a system exhibiting higher-order modes.

Finally, we explored the possibility of induction of a charge-transfer plasmon upon surface contact. This type of plasmon resonance occurs when nanospheres are close enough to allow a collective charge oscillation between the two particles.[23,24] This charge oscillation results in a time-varying total charge for each nanosphere, which is highly sensitive to the interfacial structure of the dimer.[23] Hollow gold nanospheres are ideally suited to study collective charge oscillations because they have a large interfacial volume and, therefore, are easily affected by time-dependent fluctuations in charge density. Figure 7 portrays a scheme representing the charge cloud following interaction with an EM wave having the electric field polarized parallel to the interparticle longitudinal axis of the dimer. The nanospheres of the dimer are coupled within the near-field limit. Therefore, the two surfaces in the contact zone will be instantaneously polarized with opposite signs for the charge, enhancing the stability of the charge-transfer motif. This model is consistent with the experimentally observed (Figure 4A) and theoretically confirmed (Figure 4B) thickness dependence of the SPR shift. As the spatial separation between the cavities decreased (thinner shell), the coupling strength increased. This effect appears to be responsible for the large thickness dependence we observe both theoretically and experimentally, thus pointing to a key role for local nanoparticle structural properties in determining plasmonic behavior.

At present, the contribution of asymmetric hybridized plasmon modes cannot be excluded as a contributing mechanism for the observed blue shifting of the SPR of contact HGNs. However, taken together, the strong shell thickness dependence and the absence of higher-order plasmon frequencies in the aggregate absorption spectra suggested that a charge-transfer plasmon resonance was operative in HGN contact dimers. More insight will be gained by studying these unique plasmon-supporting hollow nanospheres using advanced spectroscopic techniques and rigorous quantum mechanical treatments.

Conclusions

We have performed detailed and systematic experimental and computational studies of SPR properties for both small and extended HGN aggregates. We demonstrated that the SPR spectral position of HGN aggregates could be tuned to either higher or lower frequencies than those characteristic of the isolated HGNs. This effect, which is not observed in solid nanospheres, appears to be unique to the very thin plasmonic shells studied here. Our data indicated that the SPR blue shift that depended strongly on HGN shell thickness and aspect ratio was attributed to interparticle coupling through a charge-transfer plasmon. Additionally, the direction of the SPR shift (red or blue) was dictated by the interparticle gap separating the HGN dimers. All examined aggregates that possessed a large gap (1.2 ± 0.7 nm) showed a broad and red-shifted SPR peak, which was fully described by symmetric bonding plasmon modes. However, aggregation of thin-shell, high-aspect-ratio HGNs using short-chain dithiols exhibited a pronounced, newly formed longitudinal SPR that was blue-shifted with respect to the transverse SPR of isolated HGNs. Aggregates of low-aspect-ratio particles formed by the same manner did not show any significant spectral change. FDTD simulations reproduced the experimental measurements and also indicated that the resultant nanoscale electric field amplitudes and spatial profiles were extremely sensitive to nanosphere shell thickness. These findings highlight the critical role of the inner HGN cavity surface in composite nanostructures. Moreover, HGNs provide a versatile platform not only for plasmonic engineering but also for developing coupled composite plasmonic nanostructures.

Acknowledgment. K.L.K. gratefully acknowledges the U.S. Air Force Office of Scientific Research for financial support through the Young Investigator Program, grant no. FA9550-10-1-0300. The authors gratefully acknowledge Dr. Stephan Link for helpful discussions.

Supporting Information Available: Detailed synthetic protocol, simulation parameters, TEM structural analysis, absorption spectra, and aggregate size distributions. This material is available free of charge via the Internet at http://pubs.acs.org.

JA106910X